Design Optimization of the Biomimetic Undulating Fin of a Knife Fish Robot

Submitted: 27th August 2015; accepted 9th November 2015

Ajith Anil Meera, Attadappa Puthanveetil Sudheer

DOI: 10.14313/JAMRIS_1-2016/4

Abstract:
Median Paired Fin Propulsion used by fishes like knife fish, has the potential to replace current energy inefficient underwater propulsion systems. This paper quantizes the efficiency of a fin mechanism based on its ability to incorporate a large number of undulations. Characteristic ellipses of a mechanism were defined, based on which two algorithms were defined to measure the capabilities of the mechanism. The available workspace of the mechanism was optimized to accommodate the undulation requirements of the robot based on the formulations. Further, the distortion effect on the waveform was identified and the optimization was redefined to obviate its possibility while in operation.

Keywords: *mechanism, underwater robot, propulsion, optimization, biomimetic design, fish robot*

1. Introduction

The propulsion systems adopted by fishes and other underwater organisms might not be optimal, but they have evolved over a long period, improving and adapting on the energy utilization for locomotion. Median Paired Fin (MPF) propulsion system used in knife fish, cuttlefish etc. is one such propulsion in which the fish generates a sinusoidal waveform on its fins creating forward thrust for locomotion. Researchers have identified the potential of such systems as a replacement for the contemporary thruster based propulsion systems which are energy inefficient in nature.

Underwater robotics is a well explored field of research, while the bio-inspired underwater robotics is a less explored one. Researches have led to the development of a variety of underwater robots that emulate a real fish. The fish robot named RoboTuna, replicating the real fish with caudal and pectoral fins was developed by Barrett [1]. A soft robotic fish was developed by MIT [2] that works with fluidic elastomer actuators. Nanyang Technological University's Knife fish robot, Squid type vehicle from Osaka University, Festo's Airacuda and Stingray robot are some other examples of such robots.

The research on MPF propulsion robot include modelling and parametric study on knife fish robot by [3] and [4], kinematic modelling and dynamic analysis on the undulating fin by [5], braking performance of the squid like robot by [6], kinematic analysis of robot with two undulating fins by [7] and mechanical properties of the undulating proposer by [8]. The computational fluid dynamic analysis of the fish robot was done in [9], while [10] quantified the thrust efficiency of the robotic fish. The modelling of the motion of a biomimetic underwater vehicle was done in [11].

The potential of the MPF mode of propulsion system is immense in underwater locomotion, which makes it necessary to optimize the design. This work mainly focusses on the design optimization of the undulating fin so that the fin is capable to generate more number of undulations without any wastage in membrane extension. This work quantify the efficiency of the fin mechanism in generating more waves.

2. Mechanism

The mechanism to generate sinusoidal waveform on the fin membrane consists of a series of five bar mechanism with a flexible coupler, arranged adjacent to each other as proposed in [4].

2.1. Kinematic Design

Fig. 1 represents the mechanism, where A and D denote the center of the adjacent servo heads, BC represents the slider or flexible membrane, AB and DC represents the cranks. A number of servo motors are arranged in the line joining A and D such that the distance between the adjacent servo heads is L. The crank length is denoted by R and is same for all servos. The minimum and maximum lengths of the slider or flexible membrane is denoted by C_{min} and C_{max}.

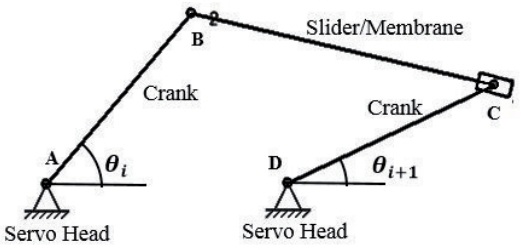

Fig. 1. Mechanism to generate sinusoidal waves

2.2. Workspace

The flexible membrane in the five bar mechanism allows the cranks to rotate independent of each other within a certain limit. The restriction over the independent movement of the cranks depends on the allowable extension of the membrane. The membrane begins to slack once the distance BC is less than C_{min}. Similarly, the membrane begins to break once the dis-

tance BC is more than C_{max}. Therefore, there exists an available workspace for the fin mechanism as given in [3]. The boundary of the workspace is represented by two hyperbolas, one representing the C_{min} hyperbola and the other, the C_{max} hyperbola. Equation (1) represent the boundary hyperbola where θ_i and θ_{i+1} are the crank angles of the ith and (i+1)th servo. The equation represents an approximate boundary of the workspace for lower values of θ_i and θ_{i+1}. The error in the equation increases with the increase in values of the crank angles.

$$\theta_i{}^2\left(1+\frac{L}{R}\right)+\theta_{i+1}{}^2\left(1-\frac{L}{R}\right)-2\theta_i\theta_{i+1}+\left(\frac{L^2-C^2}{R^2}\right)=0 \quad (1)$$

The region between both the curves represented by $C=C_{min}$ and $C=C_{max}$ is the total available workspace of the mechanism.

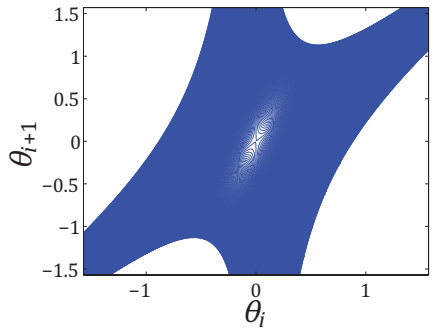

Fig. 2. Workspace of the mechanism

The joint trajectories of the adjacent crank angles making up the total available workspace for the operation of the fin where L=5, R=5, C_{min}=3 and C_{max}=8 is represented by Fig. 2., where the axes are in radians. The dimensions of the robot, taken in the paper, is chosen randomly for the purpose of illustration.

3. Undulation

The robot propels under water by creating undulations on the fin that pushes water to either side, creating a net thrust in the forward direction. The undulations used by most of the aquatic organisms for propulsion are constant amplitude undulation and linearly increasing amplitude undulation. The sinusoidal waveform is thus generated on the fin for propulsion. The fabricated model of the undulating fin of the knife fish robot is shown in Fig. 3.

Fig. 3. Undulating fin

Consider the motion of the ith and i+1th crank of a constant amplitude undulating fin.

$$\theta_i = \theta_m \sin(2\pi ft + (i-1)\beta) \quad (2)$$

$$\theta_{i+1} = \theta_m \sin(2\pi ft + i\beta) \quad (3)$$

Here i=1,2,3,....N where N is the number of servo motors used. Simplification of (2) and (3) yields (4), which represents the equation of a family of ellipses bounded inside a square for a constant θ_m.

$$\theta_i{}^2 + \theta_{i+1}{}^2 - 2\theta_i\theta_{i+1}\cos\beta - \theta_m{}^2(\sin\beta)^2 = 0 \quad (4)$$

Here θ_m and β represents the maximum amplitude and the phase difference between the adjacent crank angles, respectively. Similarly, for linearly increasing amplitude undulations, the equations are given by (5) and (6), which on simplification yields the family of ellipses bounded inside a rectangle and is represented by equation (7).

$$\theta_i = i\,\theta_m \sin(2\pi ft + (i-1)\beta) \quad (5)$$

$$\theta_{i+1} = (i+1)\,\theta_m \sin(2\pi ft + i\beta) \quad (6)$$

$$\theta_i{}^2\left(1+\frac{1}{i}\right)^2 + \theta_{i+1}{}^2 - 2\theta_i\theta_{i+1}\cos\beta\left(1+\frac{1}{i}\right) - (\theta_m(i+1)\sin\beta)^2 = 0 \quad (7)$$

4. Feasibility of an Undulation by the Mechanism

An undulation is said to be feasible by a fin mechanism if the ellipse corresponding to the undulation completely lies inside the pair of hyperbola representing the mechanical constraints offered by the membrane. The result is illustrated in Fig. 4 for L=7, R = 5, C_{min} = 5, C_{max} = 10, $\beta = 50^0$ and $\theta_m = 55^0$, where axes are in radians.

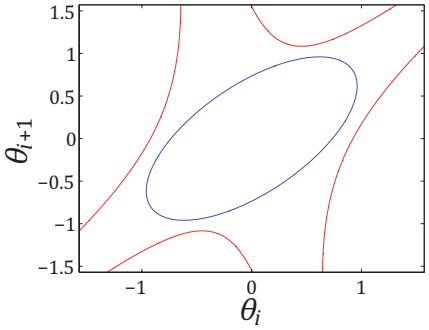

Fig. 4. Feasible undulation

4.1. Constraints over Undulation

The mechanical limitations of the five bar linkage mechanism with an extendable coupler, offers several constraints to the undulation motion produced by the knife fish robot. It imposes a restriction over the maximum amplitude of the wave generated and also over the phase difference between the sinusoidal motion of the adjacent cranks of the robot. These restrictions need to be taken care of before the generation of the wave. The phase difference of the wave has to be com-

promised to optimize the maximum amplitude of the wave. This leads to the introduction of more number of servo motors to obtain a nearly full wave. Thus, the length of the robot increases.

Selection of the maximum amplitude closer to 90^0 is possible, since one of the asymptotes of the hyperbolas is same as the axis of the ellipse. This property ensures the growth of the ellipse along the asymptote of the hyperbolas, making the undulation possible. The operational range for β will be very low if the maximum amplitude of the wave is selected closer to 90°.

5. Characteristic Ellipses of the Workspace

The term area ratio that tried to denote the usable area of the workspace was introduced by Low [3]. The ratio merely serves as a proper measure for the usable area since a square that fits in the workspace doesn't represent the actual usable workspace which is the area between the curves. Hence it serves as an imperfect measure of the usable area which is easily visible from the low values of the area ratio obtained. Moreover, it does not consider the possibility of optimizing the maximum amplitude. This incomplete representation of the usable area in the workspace by a square was redefined by introducing two new curves characterizing the workspace. The curves being the first touch ellipse for constant amplitude approach and the same for constant phase difference approach.

6. Constant Amplitude Approach

The amplitude is kept constant and the phase difference is varied to locate the intersection of the ellipse and the hyperbola.

6.1. Algorithm

The characteristic ellipses are found by iterating the values of θ_m and β, and checking for the intersection of the ellipse and the hyperbola, for a particular workspace. Initially a very low value of θ_m closer to 0^0 is chosen and β is varied from 0 to $\frac{\pi}{2}$ until the ellipse touches the hyperbola. If no intersection is detected maximum allowable phase difference is $\frac{\pi}{2}$. Since the undulations made by $\beta=\frac{\pi}{2}$ does not generate a sinusoidal profile on the fin, this region is not considered in the paper. The value of θ_m is given a small increment and the full range of β is inspected for the touch of ellipse with the hyperbola. The ellipses corresponding to this iteration can be imagined to be bounded within a square. The algorithm for the case of a constant amplitude undulation can be visualized as an expanding square centered at origin, having a set of ellipses contained within each of the growing squares. The ellipses in the squares are such that they fall inside the boundary curves represented by the C_{min} and C_{max} hyperbolas.

The growing boundary is a rectangle for a linearly increasing amplitude undulation, and the ellipses are the joint trajectories of the last pair of cranks. All the ellipses fall inside their corresponding bounding rectangle and the C_{min} and C_{max} hyperbolas. The visualization of the algorithm for constant amplitude wave for L=5, R=5, C_{min}=3 and C_{max}=7 is represented in Fig. 5, where axes are in radians.

6.2. First Touch Ellipse

The algorithm gives $\beta_{max}=\frac{\pi}{2}$ for lower values of θ_m. There exists a value of θ_m beyond which β_{max} is no longer $\frac{\pi}{2}$, but a lower value. The ellipse corresponding to the first touch on any of the pair of hyperbolas is

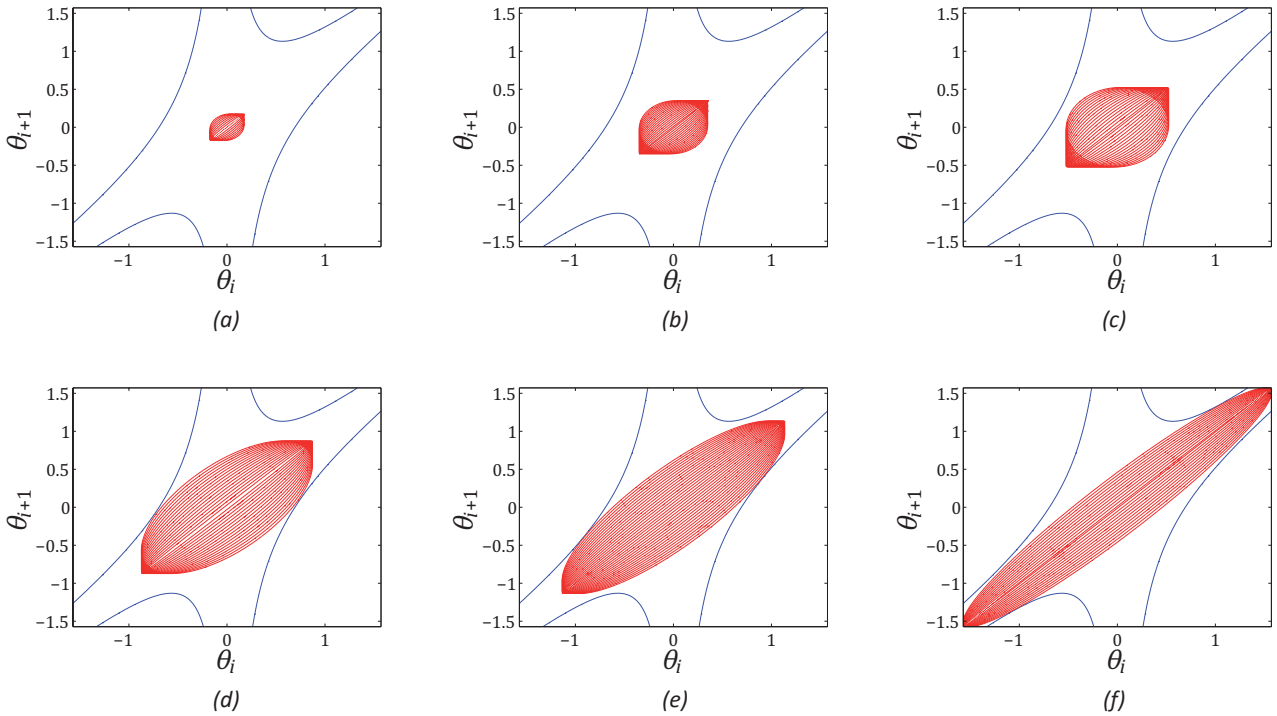

Fig. 5. Illustration of algorithm by constant amplitude approach

called the first touch ellipse. This ellipse marks the boundary of unconstrained selection of β. The value of β for the undulation is constrained as θ_m increases beyond this ellipse. Hence, the first touch ellipse of a workspace represents the boundary for unconstrained undulation. The first touch ellipse may represent the intersection of the ellipse with C_{min} or C_{max} hyperbola depending on the workspace.

6.3. Second Touch Ellipse

The constraints over β selection increase beyond the first touch ellipse. The ellipse may touch the other pair of hyperbola for the first time depending on the workspace. This ellipse that represents the first touch on the second pair of hyperbola is called the second touch ellipse. The β selection is over-constrained beyond the second touch ellipse. The ellipses tend to be congested along the common asymptote of the hyperbolas as shown in Fig. 5.

7. Constant Phase Difference Approach

The phase difference is kept constant and the amplitude is varied to check for the touch of ellipse and hyperbola.

7.1. Algorithm

A very low value of β is chosen initially and the value of θ_m is varied until the ellipse first intersects the hyperbola. This procedure is iterated for all β and the maximum allowable θ_m was found. The algorithm can be visualized as an ellipse that grows along the common asymptote of the hyperbola, with the lengths of major and minor axes growing linearly with an increase in θ_m. The ellipse takes the shape of a circle as β approaches the maximum value. The visualization of the algorithm for constant phase difference wave for L=5, R=5, C_{min}=3 and C_{max}=7 is shown in Fig. 6, where axes are in radians.

7.2. Constant Amplitude Undulation

The algorithm defined in section 6.1 and 7.1 for L=5, R=7, C_{min}=3, C_{max}=9 for a constant amplitude undulation is shown in Fig. 7 and Fig. 8, where axes are in degrees. Points A and C represent the first touch ellipses for the two approaches, while points B and D represent the second touch ellipses. The ellipses represented by A and C are the characteristic of the workspace with respect to constant amplitude undulation. Hence, the first touch ellipses of both the approaches are the characteristic ellipses and it serves as a basis of comparison between the workspaces. Ellipse with conditions at point A represents the boundary for unconstrained phase difference and ellipse with conditions at point C represents the boundary for unconstrained amplitude. The size of these ellipses vary depending on the workspace.

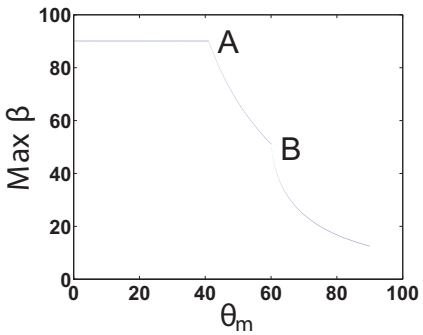

Fig. 7. Constant amplitude approach

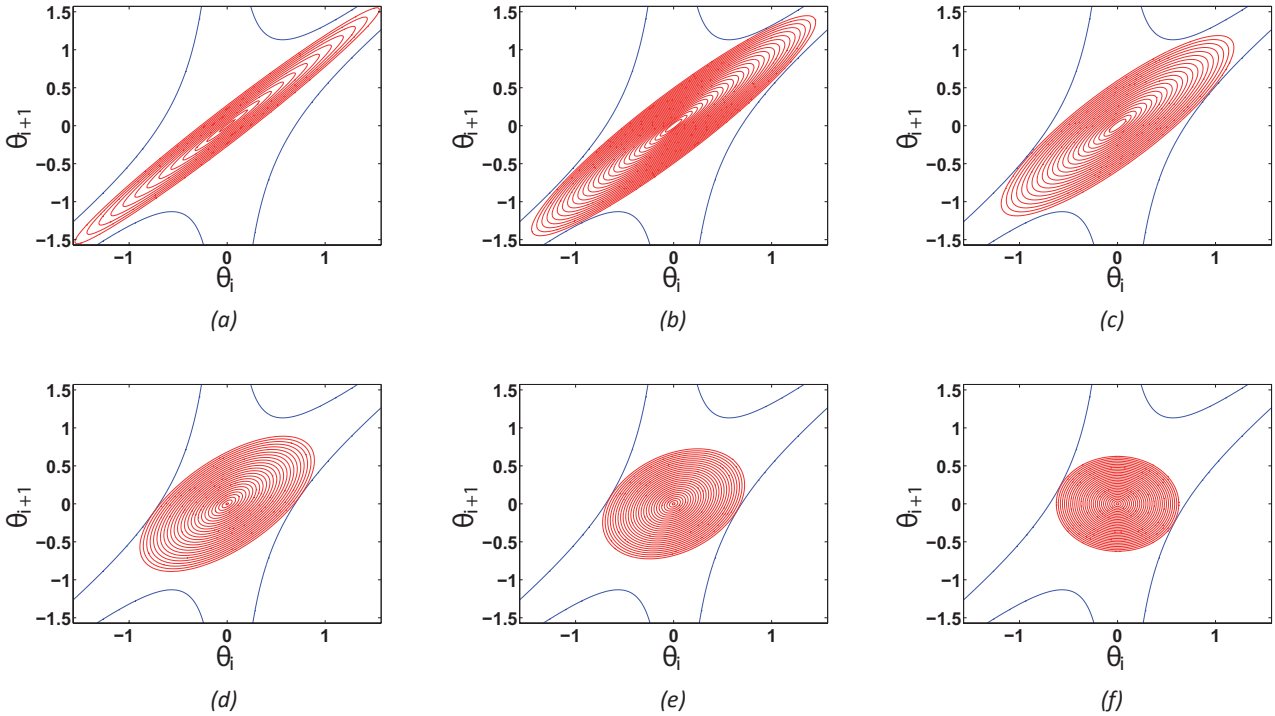

Fig. 6. Illustration of algorithm by constant phase difference approach

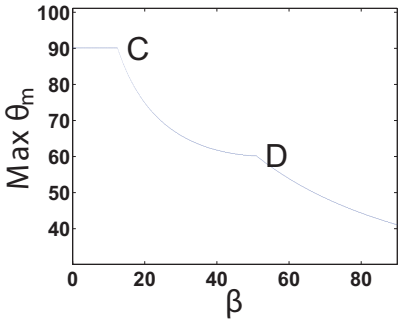

Fig. 8. Constant phase difference approach

7.3. Linearly Increasing Amplitude Undulation

The algorithm defined at section 6.1 and 7.1 for L=5, R=7, C_{min}=3, C_{max}=9, N=8 for a linearly increasing amplitude undulation is shown in Fig. 9 and Fig. 10, where axes are in degrees. The ellipse under consideration is the one corresponding to the last pair of adjacent cranks (cranks 7 and 8 in this case); the outermost ellipse of the joint trajectory. The axes of the ellipses change with θ_m and hence the ellipse does not grow about the common asymptote of the hyperbolas. Hence, the amplitude might not take its maximum value initially for the constant phase difference approach. It gets restricted to a value below $\frac{\pi}{2}$, unlike the case of a constant amplitude wave.

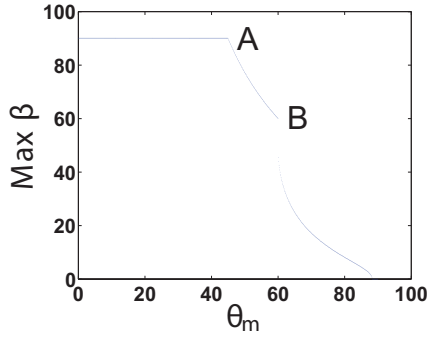

Fig. 9. Constant amplitude approach

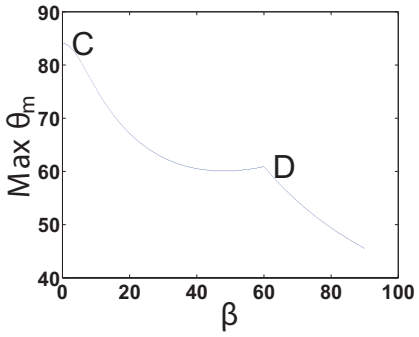

Fig. 10. Constant phase difference approach

8. Efficiency of the Mechanism for Undulation

The area contained between the hyperbolas does not represent the efficiency of a mechanism for undulation since the constant amplitude undulation has a fixed axis ellipse and hence some of the area within the workspace remains unused by the undulation. Moreover, different types of undulations use up the workspace in different manner. Hence, there is a necessity for the introduction of an efficiency term, defined based on the undulation to be generated. The usable area of the workspace created by a mechanism for an undulation was quantized by introducing two efficiencies, one based on the first touch ellipse on constant amplitude approach and the other on constant phase difference approach.

8.1. Constant Amplitude Undulation

The unconstrained phase difference efficiency, η_p is defined as the ratio of the area of the first touch ellipse from constant amplitude approach to the total available workspace area. The unconstrained amplitude efficiency, η_a is defined as the ratio of the area of the first touch ellipse from constant phase difference approach to the total available workspace area. A higher value of η_a represent the better capability of a mechanism to incorporate waves of higher amplitude, without any constraints on the phase difference. Similarly, a higher value of η_a represent the capability to generate waves of higher phase difference without any constraints on the amplitude selection. As per the requirement of the swimming performance of the robot, an optimum value of both the efficiencies can be selected.

It can be noted that $\beta = \frac{\pi}{2}$ for the first touch ellipse for constant amplitude approach and, $\theta_m = \frac{\pi}{2}$ for the first touch ellipse for constant phase difference approach.

Area of first touch ellipse (constant amplitude approach): $A_1 = \pi {\theta_m}^2$.

Area of first touch ellipse (constant phase difference approach): $A_2 = \frac{1}{4}\pi^3 \sin\beta$.

Area of total available Workspace for servos: $A_3=\pi^2$.

$$\eta_p = \frac{A_1}{A_3} \times 100 = \frac{100{\theta_m}^2}{\pi} \tag{8}$$

$$\eta_a = \frac{A_2}{A_3} \times 100 = 25\pi \sin\beta \tag{9}$$

The maximum possible efficiency is 78.54%.

8.2. Linearly Increasing Amplitude Undulation

Unlike the case of constant amplitude undulation, the unconstrained amplitude selection might not be possible in some mechanisms. Hence, the first touch ellipse for constant phase difference approach has a restricted θ_m even for a very low β. Similar to the constant amplitude undulation, $\beta = \frac{\pi}{2}$ for the first touch ellipse for constant amplitude approach.

Area of first touch ellipse (constant amplitude approach): $A_1 = i(i+1)\,\pi {\theta_m}^2$.

Area of first touch ellipse (constant phase difference approach): $A_2 = i(i+1)\,\pi {\theta_m}^2 \sin\beta$.

Area of total available Workspace for servos: $A_3=\pi^2$.

$$\eta_p = \frac{100i(i+1){\theta_m}^2}{\pi} \tag{10}$$

$$\eta_a = \frac{100\,i(i+1){\theta_m}^2 \sin\beta}{\pi} \tag{11}$$

9. Optimal Workspace Design

It is necessary that the robot is capable to perform a variety of undulations with different amplitudes and phase differences, for the optimum performance of a fish robot. An increase in the workspace of the mecha-

nism increases the variety of undulations the fish is capable to perform. Moreover, the experimental results [4] of a knife fish robot, shows an optimal value for the phase difference in order to obtain maximum velocity in the forward direction. The robot should be capable to perform these optimum undulations.

The ellipses in section 6 are stepwise bounded by a square corresponding to the chosen θ_m . The optimum workspace design corresponds to the touch of the C_{min} hyperbola with the top and bottom sides of the square and the touch of the C_{max} hyperbola with the circle corresponding to the maximum phase difference for a given amplitude. Hence, the optimum design for a given η_p is such that one pair of hyperbola touches the bounding square and the other pair touches the circle inscribed in the bounding square as shown in Fig. 11, where axes are in radians. The design ensures an unrestricted amplitude choice below the design value and an unrestricted phase difference choice below $\frac{\pi}{2}$.

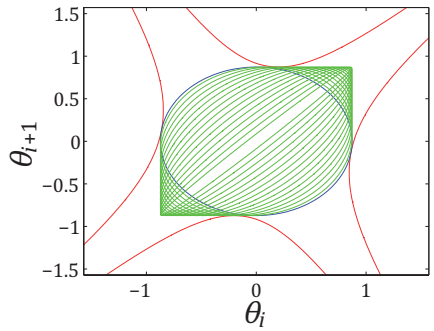

Fig. 11. Optimum workspace

For such an optimal design of the mechanism, the ellipse for constant amplitude approach first touches both the pairs of hyperbolas simultaneously. This eliminates the existence of a second touch ellipse. Hence, in an optimum workspace design, the second touch ellipse should coincide with the first touch ellipse. This selection eliminate the wastage of the membrane extension and reduce the need for high quality membrane.

The workspace design procedure starts with the selection of η_p as per the requirement. Corresponding to a η_p, there exists a bounding square and an inscribed circle for constant amplitude undulation. The pairs of hyperbolas are selected such that one pair touches the bounding square and the other touches the inscribed circle. The equation of the inscribed circle is given by equation (12).

$$\theta_i^{\,2} + \theta_{i+1}^{\,2} = \theta_m^{\,2} \tag{12}$$

Solving the hyperbola, inscribed circle and the bounding square gives equations (13) and (14) that represent the optimal workspace design.

$$\left(\frac{C_{max}}{R}\right)^2 = \left(\frac{L}{R}\right)^2 + \theta_m^{\,2}\left(1 + \sqrt{1 + \left(\frac{L}{R}\right)^2}\right) \tag{13}$$

$$\left(\frac{C_{min}}{R}\right)^2 = \left(\frac{L}{R}\right)^2 - \frac{\theta_m^{\,2}\left(\frac{L}{R}\right)^2}{1+\frac{L}{R}} \tag{14}$$

It can be concluded that, for achieving a η_p for a selected L/R>1, the optimum slider lengths are fully defined from equation (13) and (14). The blue colored circle in Fig. 11 represents the inscribed circle for the set of all waves corresponding to amplitude of 50^0. The design of the slider for L/R=3.3 is computed using the algorithm mentioned above and is represented by the red colored hyperbolas in Fig 11. Hence, this design procedure ensures the feasibility of the undulations below a design amplitude. The membrane is chosen based on this approach. Hence, the design procedure of the undulating fin is such that it considers all the undulations that the mechanism is supposed to produce, without any wastage in elongation.

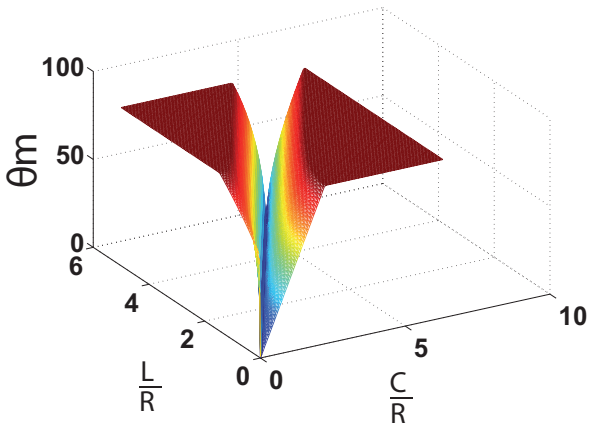

Fig. 12. Workspace Optimization Surface

The surface for equation (13) for $\frac{C}{R} > \frac{L}{R}$ and equation (14) for $\frac{C}{R} < \frac{L}{R}$ is shown in Fig 12. In case of a constant L/R, θ_m decreases for an increasing $\frac{C}{R}$ until $\frac{C}{R} = \frac{L}{R}$ and then increases with $\frac{C}{R}$. Similarly, for a constant $\frac{C}{R}$, θ_m decreases for an increasing $\frac{L}{R}$ until $\frac{C}{R} = \frac{L}{R}$ and then increases with $\frac{L}{R}$. The plateau surface corresponding to the lower values of L/R and higher values of C/R and vice versa in the Fig 12 represents the saturated θ_m region. C_{min} and C_{max} should be chosen such that they lie on the opposite sides of the line $\frac{C}{R} - \frac{L}{R} = 0$ and on the intersection of the curves of constant θ_m plane and constant L/R plane as per the design requirement. Optimizing θ_m ensures the complete flexibility in selection of the phase difference.

The increase in elongation of the slider/membrane as θ_m increases can be observed from Fig. 12. It can be visualized as the widening up of the two curves from their line of intersection as shown in Fig. 12. Hence choosing a lower θ_m will reduce the need for higher elongation of the membrane/slider.

10. Distortions in the Generated Wave

The analysis done so far is with the assumption that a sine wave profile is generated on the fin membrane when the adjacent cranks are rotated in a specific pattern as mentioned in the beginning. However, there are some special cases where a sine wave profile might not exactly be generated, maybe for a specific period of time in each cycle. This factor has not been considered by any previous research in this field.

Consider a mechanism with L<R, during the operation of the fin, there is a possibility that at any instant, the mechanism takes a form similar to the one

in Fig. 13 where crank end B of the i^{th} servo crosses the crank end of $(i+1)^{th}$ servo. In such cases, the slider/membrane curves back and forms distortions in the sine wave at that instant. This phenomenon may lead to vortex formation or turbulence in water at that instant and consumes more power to propagate under water. Also it may lead to the instability of the robot giving non uniform forward thrust. Hence, it is necessary to preclude such distortions through optimal design.

Such a distortion happens when, $L+R\cos\theta_{i+1} \geq R\cos\theta_i$ or $\frac{L}{R} \geq \cos\theta_i - \cos\theta_{i+1}$. The Taylor series approximation of the expression reduces to equation (15) which is the expression for a hyperbola.

$$\frac{2L}{R} \geq {\theta_{i+1}}^2 - {\theta_i}^2 \tag{15}$$

Hence, for $L<R$ the family of ellipses should lie inside three pair of hyperbolas. The optimized workspace will correspond to the touch of the distortion hyperbola to the top and bottom of the bounding square, and the touch of inscribed circle to the C_{max} hyperbola. Design of $\frac{L}{R}$ to generate a wave should obey condition (16) to prevent distortion effects during operation.

$$\theta_m \leq \sqrt{\frac{2L}{R}} \tag{16}$$

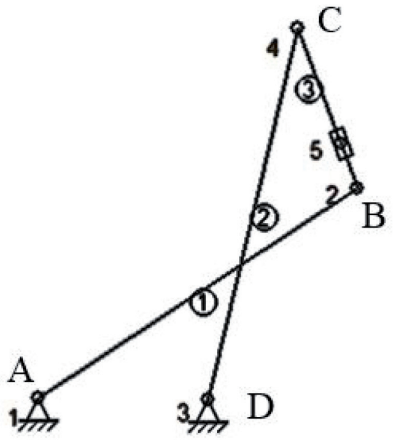

Fig. 13. Distortion in sine wave

Hence, the optimization procedure will include selection of the maximum amplitude of operation of the mechanism, determination of minimum value of $\frac{L}{R}$ from (16), and determination of $\frac{C_{max}}{R}$ and $\frac{C_{min}}{R}$ from (13) and (14). Therefore, to decrease the size of the robot, $\frac{L}{R}$ can be selected less than 1 for a maximum amplitude of up to 81.03°. The error of 9.87° is due to the error in Taylor series approximation.

The optimization for the set of all waves below 60°amplitude for unrestricted phase difference is given by Fig. 14, where $\frac{L}{R}<1$. The pink curve represents the distortion hyperbola for $\frac{L}{R}$=0,583. It can be noted that the entire green region is inside the region bounded by three pair of hyperbolas, two representing the mechanical constraints due to the membrane and one representing the distortion of the sine wave.

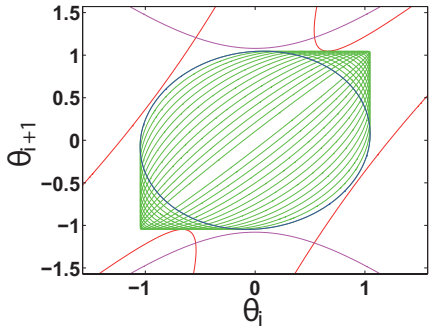

Fig. 14. Optimization in case of distortion

11. Conclusion and Outlook

The algorithms that help to compare the workspace of various fin mechanisms were introduced. The characteristic ellipses were defined for a mechanism and were used to evaluate two new efficiency terms. These parameters were used to compare the efficiency with which the mechanism is capable to incorporate wide variety of undulations.

In light of the results from the analysis, the workspace was optimized to reduce wastage of elongation of the membrane. The fin was designed based on the optimization technique employed to evaluate the parameters of the mechanism as per the requirements of the robot. A distortion effect on the sine wave generated was identified and the optimization was redefined to get rid of such distortions in the design stage itself. The optimization was done to incorporate all types of undulations, and not specifically for the most thrust generating wave.

This work can be extended in different ways. The hydrodynamic force analysis on the fin can be done with the optimum design. The wave corresponding to the maximum thrust generation is to be found and the optimization algorithm could be modified to incorporate the wave. The equations governing the interdependency of the wave generated and the stability of the robot is to be found. Energy efficiency of the fin could be evaluated to check for its better performance than thrusters. Further, this technology can be incorporated in the marine drives as it is expected to be more energy efficient than the thrusters. Future underwater robots may be made with this kind of Median Paired Fin propulsion system which could be used for oceanographic researches, underwater surveillance, swarm robotics etc.

ACKNOWLEDGMENT

This research was supported by National Institute of Technology Calicut, Kerala, India by providing laboratory facilities and funds for fabrication and experimentation of the robot. This support is gratefully acknowledged.

AUTHORS

Ajith Anil Meera* – Robotics Interest Group, Department of Mechanical Engineering, National Institute of Technology, Calicut, Kerala, India-673601. Tel. +918547267258.

E-mail: ajitham1994@gmail.com.

Attadappa Puthanveetil Sudheer – Department of Mechanical Engineering Robotics\Mechatronics Lab National Institute of Technology, Calicut Kerala, India-673601. Tel. +919961450987

E-mail: apsudheer@nitc.ac.in

*Corresponding author

REFERENCES

[1] Triantafyllou M.S., Yue D. K. P., Grosenbaugh M. A., Wolfgang M. J., Barrett D. S., "Drag reduction in fish like locomotion", *Journal of Fluid Mechanics*, 1999, vol. 392, 83–212. DOI: 10.1017/S0022112099005455.

[2] Onal C.D., Rus D., Marchese A. D., "Autonomous Soft Robotic Fish Capable of Escape Maneuvers Using Fluidic Elastomer Actuators", *Soft Robotics*, 2014, vol. 1, no. 1, 75–87. doi:10.1089/soro.2013.0009.

[3] Low K.H, "Modelling and parametric study of modular undulating fin rays", *Mechanism and Machine Theory*, 2009, vol. 44, no. 3, 615–632. DOI:10.1016/j.mechmachtheory.2008.11.009

[4] Low K.H, Willy A., "Biomimetic Motion Planning of an Undulating Robotic Fish Fin", *Journal of Vibration and Control*, 2006, vol. 12, no. 12, 1337–1359. DOI: 10.1177/1077546306070597.

[5] Lincheng Shen, Tianjiang Hu, Guangming Wang, "Kinematic Modeling and Dynamic Analysis of the Long-based Undulation Fin", *Icarv*, 5-8 Dec. 2006, 1–6. DOI: 10.1109/ICARCV.2006.345111.

[6] Sugimori S., Miki H., Yamamoto R., et al., "Braking Performance of a Biomimetic Squid-Like Underwater Robot", *Japan Journal of Bionic Engineering*, 2013, vol. 10, no. 3, 265–273. DOI: 10.1016/S1672-6529(13)60222-X.

[7] Wang S., Dong X., Shang L.-J., et al., "Design and Kinetic Analysis of a Biomimetic Underwater Vehicle with Two Undulating Long-fins", *Acta Automatica Sinica*, 2013, vol. 39, no. 8, 1330–1338. DOI: 10.1016/S1874-1029(13)60049-X.

[8] Patankar N. A., Lauder G. V., MacIver M. A., Curet O. M., "Mechanical properties of a bio-inspired robotic knifefish with an undulatory propulsor", *Bioinspiration and Biomimetics*, April 2011, vol. 6, no. 2. Doi:10.1088/1748-3182/6/2/026004.

[9] Lamas M. I., J. D. Rodriguez, C. G. Rodriguez, "CFD Analysis of Biologically Inspired Marine Propulsors", *Brodogradnja*, 2012, vol. 63, no. 2, 125–133.

[10] Tianmiao Wang, Guanhao Wu, and Jianhong Liang Li Wen, "Quantitative Thrust Efficiency of a Self-Propulsive Robotic Fish: Experimental Method and Hydrodynamic Investigation", *IEEE/ASME Transactions on Mechatronics*, June 2013, vol. 18, no. 3, 1027–1038. DOI: 10.1109/TMECH.2012.2194719

[11] Morawski M., Malec M., Szymak P., Trzmiel A., "Analysis of Parameters of Traveling Wave Impact on the Speed of Biomimetic Underwater Vehicle", *Solid State Phenomena*, vol. 210, 273–279, Oct. 2013, DOI: 10.4028/www.scientific.net/SSP.210.273.